Attosecond counter-rotating-wave effect in xenon driven by strong fields

M. Anand,[1,2] Stefan Pabst,[3] Ojoon Kwon,[1,2] and Dong Eon Kim[1,2,*]

[1]*Department of Physics, Center for Attosecond Science and Technology, POSTECH, 77 Cheongam-Ro, Nam-Gu, Pohang, Gyeongbuk 37673, Republic of Korea*

[2]*Max Planck Center for Attosecond Science, Max Planck POSTECH/KOREA Research Initiative, 77 Cheongam-Ro, Nam-Gu, Pohang, Gyeongbuk 37673, Republic of Korea*

[3]*ITAMP, Harvard-Smithsonian Center for Astrophysics, 60 Garden Street, Cambridge, Massachusetts 02138, USA*

(Received 21 October 2016; revised manuscript received 20 January 2017; published 26 May 2017)

We investigate the subfemtosecond dynamics of a highly excited xenon atom coherently driven by a strong control field at which the Rabi frequency of the system is comparable to the frequency of a driving laser. The widely used rotating-wave approximation breaks down at such fields, resulting in features such as the counter-rotating-wave (CRW) effect. We present a time-resolved observation of the CRW effect in the highly excited $4d^{-1}np$ xenon using attosecond transient absorption spectroscopy. Time-dependent many-body theory confirms the observation and explains the various features of the absorption spectrum seen in experiment.

DOI: 10.1103/PhysRevA.95.053420

I. INTRODUCTION

The manipulation of atoms, molecules, and solids and the interest in electron dynamics in strong fields have been long standing. Much attention has been recently paid to radically new optical and electrical properties such as electromagnetically induced transparency (EIT) [1,2], redshifted optical absorption [3], high-order harmonics generation (HHG) [4–7], and semimetallization [8–10]. We have just begun to understand the strong-field response of various forms of materials. In analysis of light-matter interaction, the rotating-wave approximation (RWA) has been widely used, which holds as long as the Rabi frequency, which is proportional to the driving field, is much smaller than the driving frequency. For strong light-matter interaction, this approximation breaks down and the effects originating from the counter-rotating terms in the Hamiltonian [11] appear. With ultrashort pulses and the development of attosecond metrology [12], it is now possible to study counter-rotating-wave (CRW) effects on a subfemtosecond time scale. These CRW effects have important consequences on the dynamics of the system and can lead to interesting applications as shown in circuit quantum electrodynamics [13], quantum computation (QC) using SQUIDS [14], and in the creation of entanglement between two atoms [15].

In this work, we report the real time observation of ultrafast subcycle CRW features with optical frequencies. We study the CRW effect in highly excited $4d^{-1}np$ states in atomic xenon, which are dressed by an intense near infrared (NIR) pulse. We probe the field-driven dressing dynamics in the $4d^{-1}np$ manifolds using an attosecond pulse delayed with respect to the IR pulse. All $4d^{-1}np$ states are autoionizing states with a lifetime of about 6.6 fs, due to the Auger decay of the unstable $4d$ hole. Consequently, the CRW has to be faster than the lifetime to be observed. For an 800-nm pulse, the optical period is 2.6 fs and the CRW effect occurs within 1.3 fs, beating several times within the core lifetime. To observe the ultrafast electron dynamics in real time, we applied attosecond transient absorption spectroscopy (ATAS) [16–21], which extends transient absorption spectroscopy to attosecond time scales. The appearing of CRW effects in ATAS has been theoretically studied [22,23] but has not been clearly seen in experiment.

ATAS experiments have focused so far on ionizing or excited outer-valence electrons [16–20]. Here, we study highly excited states with a core hole in the $4d$ shell. These states have lifetimes of only a few femtoseconds. Studying their dynamical properties with common spectroscopic approaches using quasimonochromatic pulses has not been possible. ATAS overcomes this obstacle where the attosecond extreme ultraviolet (XUV) pulses access the highly excited states and at the same time probe their dynamical response on a subcycle time scale to an intense NIR pulse [17,18,21].

II. EXPERIMENTS

The experimental setup used in our experiments is shown in Fig. 1. A carrier-envelope phase-stabilized Ti:sapphire, few-cycle laser pulse (4 fs FWHM, 800 nm, 300 μJ) is focused onto a static neon gas cell to produce HHG radiation in the XUV region. The XUV attosecond pulses generated by the process of HHG in Ne gas copropagate along with the residual NIR pulse to the main experimental chamber and are used for pump-probe studies. The details of the experimental setup are given in the Appendix.

The attosecond XUV and NIR pulse are then focused onto a target gas cell. After the gas cell, the NIR pulse is cut off using a 0.15-μm aluminum filter and only the attosecond XUV pulse is steered and focused at the entrance slit of an XUV spectrometer (see Appendix) using a spherical mirror.

The ATAS is constructed by measuring the transmitted spectrum ($I_{\rm gas}$) through the gas target (Xe) as a function of delay (τ) between NIR and XUV pulses from delays of -10 to 6 fs (negative delays correspond to XUV pulse arriving first) with a step of 200 as. Each measurement corresponds to an average taken over ~9000 shots. The absorption spectrum is calculated using the reference XUV spectrum (I_0) taken in the absence of the xenon gas target. The optical density is calculated by using the following expression,

$$\mathcal{D}_{\rm opt}(E,\tau) = \ln\left[\frac{I_{\rm gas}(E,\tau)}{I_0}\right],$$

*Corresponding author: kimd@postech.ac.kr

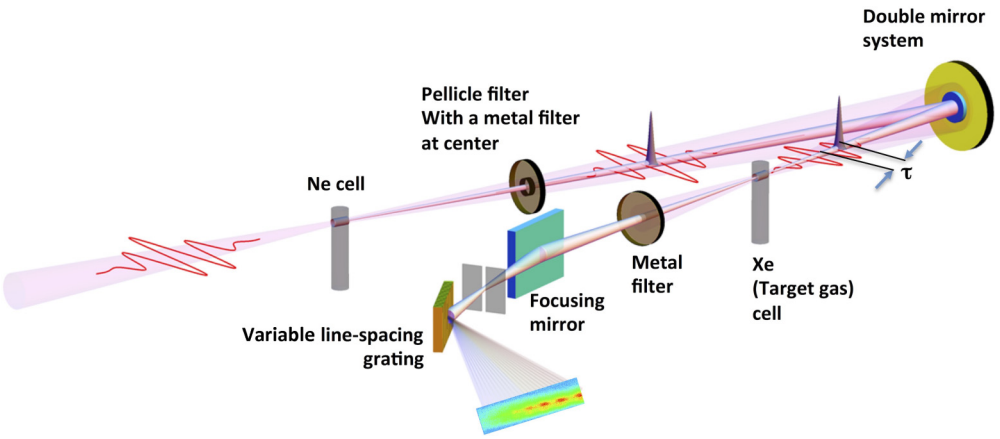

FIG. 1. Experimental setup for attosecond transient absorption spectroscopy Attosecond XUV pulses are generated from neon gas, using few-cycle femtosecond NIR pulses (4 fs, 800 nm, 0.3 mJ). A concentric two-segment curved mirror along with a special metal filter (see Appendix), separates the attosecond XUV and the NIR pulses and provides a precision delay between them. The two beams are then focused collinearly onto a quasistatic gas cell containing xenon as a target gas. The absorption spectrum is obtained by measuring the transmitted spectrum (I_{gas}) from the gas target and also a spectrum in the absence of the gas target (I_0) as a function of delay between NIR and XUV pulses.

for each delay. The raw transient absorption spectrum obtained from these raw data is then filtered and processed for greater fidelity (see Appendix) to obtain the ATAS shown in Fig 2(a).

III. RESULTS

Figure 2(a) shows the optical density measured from xenon in the spectral region of 64–70 eV as a function of delay between the NIR and XUV pulse. The intensity of the NIR field for these measurements was about 2×10^{13} W/cm^2. The absorption lines correspond to the core-electron excited states $4d_{5/2}^{-1}6p$, $4d_{3/2}^{-1}6p$, and $4d_{3/2}^{-1}7p$, as shown in Fig. 2(c). The three main features noted in the region of overlap between the pulses are (1) the splitting of the absorption lines, (2) the asymmetry in the splitting (dotted yellow line), and (3) the oscillating substructures within them. The oscillating substructures have

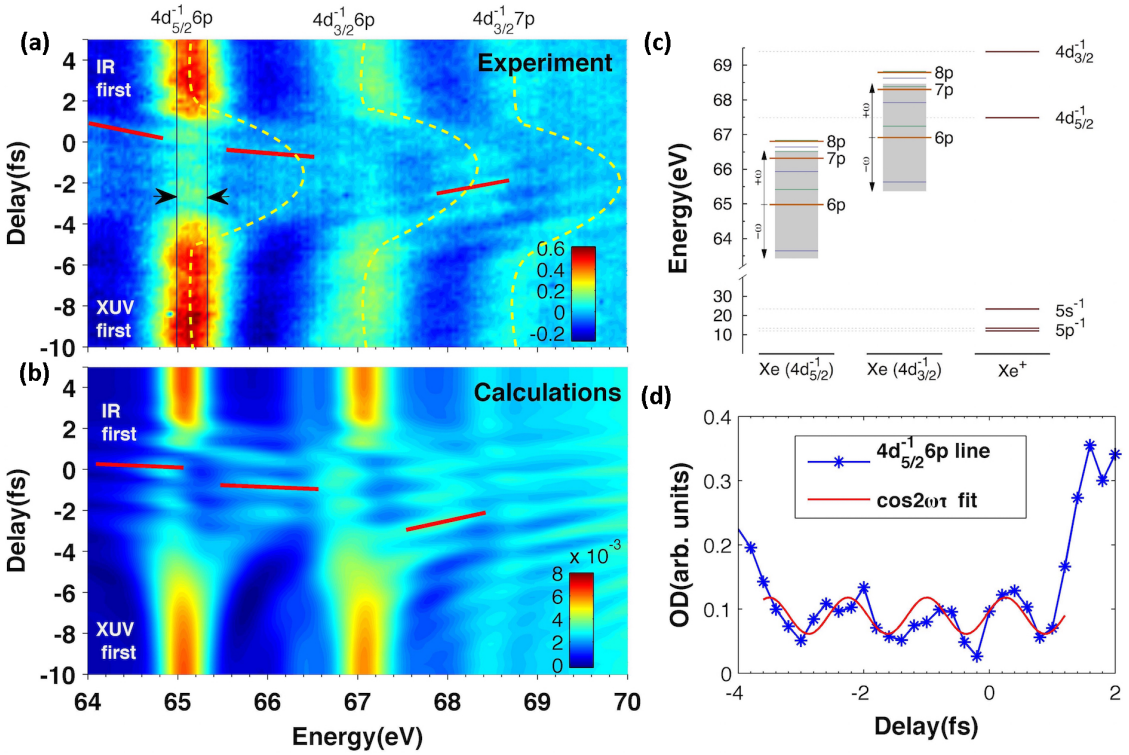

FIG. 2. Attosecond transient absorption spectrum of Xe. (a) Experimental absorption spectra at different delays between XUV and NIR pulse at NIR intensity of about 2×10^{13} W/cm^2. (b) TDCIS calculations under similar conditions. (c) Inner-shell excited states of xenon with a hole in the $4d_{5/2}$ and $4d_{3/2}$ shell. The ionization thresholds of the various shells are shown in the third column. (d) Subcycle oscillation seen at the 65-eV line ($4d_{5/2}^{-1}6p$, blue curve) in the experimental spectrum, averaged over 200 meV bandwidth shown using two black lines in (a). The cos($2\omega\tau$) fit to the experimental data is shown in red. Negative delays correspond to the arrival of an XUV pulse before an NIR pulse.

a frequency of about twice the NIR frequency. This is seen more clearly in Fig. 2(d) (blue line), where the optical density integrated over a bandwidth of 200 meV [area between the black vertical lines in Fig. 2(a)] centered at the 65 eV absorption line ($4d_{5/2}^{-1}6p$) is shown as a function of delay between the NIR and XUV pulse.

IV. SIMULATIONS AND DISCUSSIONS

We have used a time-dependent many-body approach based on configuration-interaction singles (TDCIS) [24,25] to understand the features seen in the absorption spectrum. TDCIS describes successfully many-electron atoms in the presence of strong-field pulses and has been used to understand various atomic and many-body effects at ultrashort time scales [26,27]. The absorption spectrum from the calculations was convoluted with the spectrometer resolution to compare with the experimental results. The calculations were performed assuming a Gaussian IR pulse of about 4 fs, centered at 800 nm with a peak intensity of 2×10^{13} W/cm^2 and a 200-as XUV pulse centered at 66 eV.

The calculated absorption spectrum for xenon [Fig. 2(b)] agrees well with experiment [Fig. 2(a)], showing both the subcycle oscillating features and the asymmetric Autler-Townes splitting (dotted line). The calculated absorption spectrum also reproduces the slopes for the oscillating structures [shown by red lines in Fig. 2(a)] for the $4d_{5/2}^{-1}6p, 4d_{3/2}^{-1}6p$ absorption lines. The differences in the slopes are a direct consequence of the phase difference between the different pathways involved in the interactions [28].

The most important feature seen in our experiments are the $2\omega_{\mathrm{IR}}$ oscillations of the absorption line when the NIR and XUV pulse overlap. The $2\omega_{\mathrm{IR}}$ oscillation are seen clearly in Fig. 2(d), where the $\cos(2\omega\tau)$ fit to the experimental data is shown in red. This oscillation should not exist according to the RWA but constitute the CRW effect. The $2\omega_{\mathrm{IR}}$ oscillation has been observed in earlier experiments [29,30] and has been typically understood in terms of which-way (two path) interference where the absorption of an XUV photon represents the direct pathway and the indirect pathway consists of a third-order process involving the absorption of another XUV photon plus the absorption or emission of two NIR photons. In our case, the possibility of two-path interference contributing to the subcycle oscillations is much smaller than that of the CRW effect. This can be inferred from Fig. 2(c), where the accessible states from $4d_{3/2}^{-1}6p$ and $4d_{5/2}^{-1}6p$ states by single NIR photon are shown. A two-photon process would involve continuum energy states above the $4d_{3/2,5/2}^{-1}$ ionization limit rendering the process very unlikely. Also the fact that we do not see $2\omega_{\mathrm{IR}}$ oscillations for negative delays (XUV pulse comes first) is another strong indication that which-way interference is negligible here [28,29]. Including only bound states in the calculations, so that which-way interferences are basically prohibited [see Fig. 3(a)], the simulated result reproduces the experimental observation and is another confirmation for the CRW nature of the $2\omega_{\mathrm{IR}}$ oscillations.

The origin of the counter-rotating-wave terms can be understood in a simple field-driven two-level system. The Hamiltonian in the rotating frame [31] reads

$$\hat{H} = \begin{pmatrix} \Delta & 0 \\ 0 & 0 \end{pmatrix} + \frac{\Omega}{2}\begin{pmatrix} 0 & 1 \\ 1 & 0 \end{pmatrix} + \frac{\Omega}{2}\begin{pmatrix} 0 & e^{2i\omega t} \\ e^{-2i\omega t} & 0 \end{pmatrix},$$

where $\Omega = \mu E$ is the Rabi frequency, μ is the transition dipole moment, E is the amplitude of the electric field, ω is the transition frequency, and Δ is the detuning. In the RWA, only the first two terms are kept, and the rapidly oscillating third term, which is the CRW term, is dropped. In the first-order perturbation theory for the RWA, one finds that the strength of the CRW correction is proportional to Ω/ω and oscillates with a frequency of 2ω [17,20]. Note that the strength of this term does not depend on the pulse duration [31]. Conventionally, in the optical regime, the Rabi frequency is commonly much smaller than the driving frequency, $\Omega/\omega \ll 1$. Even for a weak field, the CRW term may have a significant influence by modifying the resonance condition known as Bloch-Siegert shift [14,32] and rendering the Rabi frequency time dependent [31]. The CRW term gives rise to a second (time-dependent) pathway to excite or deexcite the system, which depending on the time t interferes constructively or destructively with the RWA pathway. This interference happens twice per cycle resulting in the 2ω modulation of the population. As the Rabi frequency Ω increases comparable to ω, the probability of excitation (deexcitation) within a quarter of an optical cycle increases as well, making CRW modulation more visible. With the emergence of intense femtosecond pulses reaching intensities above 10^{13} W/cm^2, it is nowadays possible to induce these Rabi splittings of $\sim$1 eV [33,34], breaking down RWA. Generally, large noble gas atoms possess larger dipole transition moments than light atoms favoring CRW effects. Therefore, xenon is an ideal choice for studying CRW effects. In xenon, the Rabi splitting is 1.4 eV, for resonantly driven the $4d_{5/2}^{-1}6p$ to $4d_{5/2}^{-1}6s$ transition at an intensity of 2×10^{13} W/cm^2 of laser light (photon energy of 1.3 eV), and exceeds the resonant driving frequency. The CRW effects should be consequently very prominent as Figs. 2(a) and 2(d) confirm.

To demonstrate the influence of the CRW, we focus on the $4d_{5/2}^{-1}6p$ line and perform two series of calculations: (1) varying laser intensities [Fig. 3(a)] and (2) changing driving frequency and the energy spacing between the excited states [Fig. 3(b)]. We limit ourselves to the three-level system and resonant driving frequency ω between the states $4d_{5/2}^{-1}6p$ and $4d_{5/2}^{-1}6s$ to demonstrate how the CRW depends on these variables as the ratio Ω/ω varies. By increasing the intensity, the Rabi frequency increases but the driving frequency stays the same. The visibility of the 2ω oscillations improves as the intensity increases as shown in Fig 3(a). Also the Autler-Townes splitting moves further apart and becomes spectrally broader. In xenon this is a problem, as the neighboring $4d_{3/2}^{-1}6p$ state is only 2 eV away and starts to overlap with features of the $4d_{5/2}^{-1}6p$ line. This also limits the range of useful NIR pulse intensities to observe the CRW effect.

The series in Fig. 3(b) shows the absorption spectra keeping the $4d_{5/2}^{-1}6p$ level fixed but scaling all the transition energies to the $4d^{-1}nd$ and $4d^{-1}ns$ energies by a common factor. In this way, the Rabi frequency Ω is kept constant and the driving frequency ω is varied. The energy levels and the driving

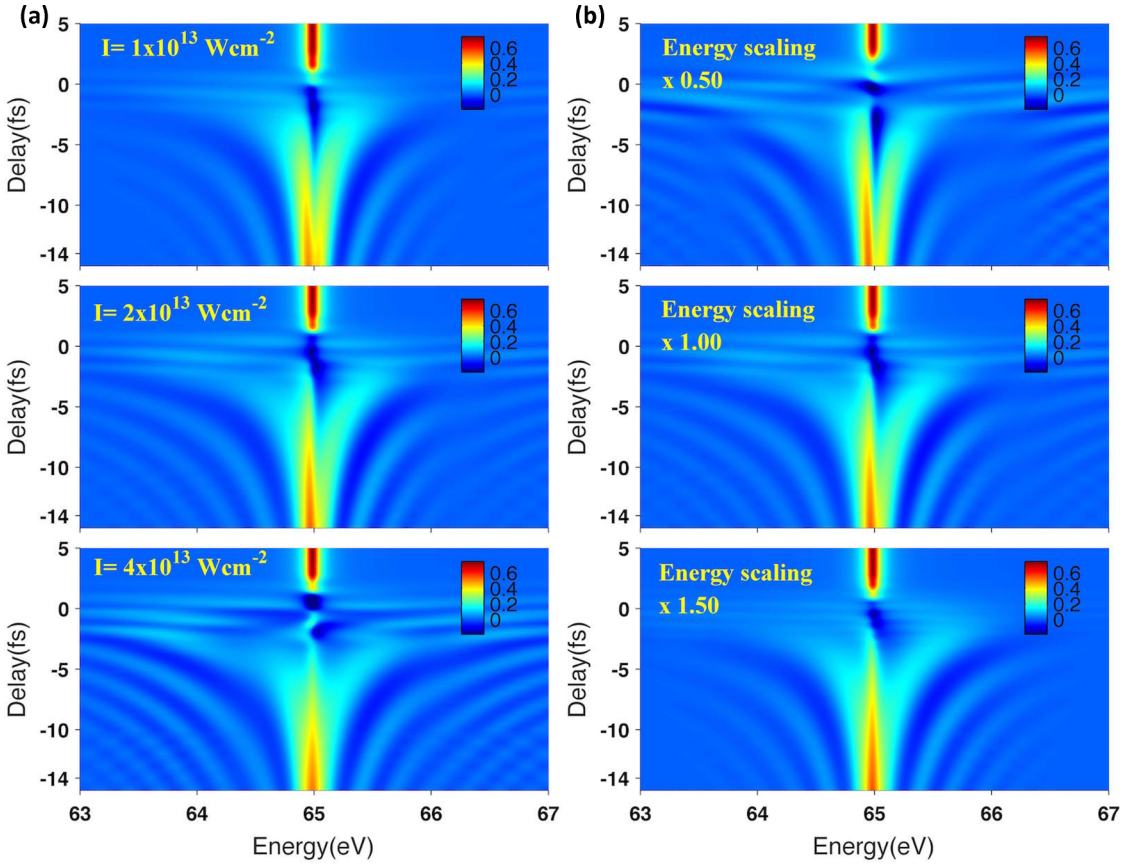

FIG. 3. Change of absorption line of the $4d_{5/2}^{-1}6p$ state for different conditions of the control field. (a) Calculations are done for different intensities ($1, 2, 4 \times 10^{13}$ W/cm^2). As the ratio of Rabi frequency to the control field frequency increases, the oscillating features become more prominent. (b) Calculations are done at a fixed intensity of 2×10^{13} W/cm^2 with scaling the separation of all the $4d_{5/2}^{-1}nd$, $4d_{5/2}^{-1}ns$ states with respect to the $4d_{5/2}^{-1}6p$ state by a factor of 0.5, 1, and 1.5. As the scaling increases, the oscillating effect diminishes considerably.

frequency are scaled by factors of 0.5, 1, and 1.5, keeping the intensity constant at 2×10^{13} W/cm^2. With increasing driving frequency, the CRW oscillations become faster and the visibility goes down due to the decreasing ratio of Ω/ω. Both trends shown in Fig. 3 are beneficial when changing the atom from neon to xenon. The ratio Ω/ω increases because Ω increases due to the larger dipole strengths between states and the energy spacing between the neighboring ns and np states slightly decreases.

Even though the CRW effect has been often discussed in the connection with short femtosecond pulses, it is not the shortness of the pulse (or broad spectrum) that leads to an enhanced CRW effect but only the large peak intensities that are possible with these short pulses. These can be seen in Fig. 4 where the ATAS is shown for few-cycle [Fig. 4(a)] and many-cycle [Fig. 4(b)] pulses, respectively. The cut along an Autler-Townes branch [black lines in Figs. 4(a) and 4(b)] is made and shown in Fig. 4(c). The 2ω oscillations are clearly seen and the strengths of the oscillations are very similar for both pulses in the region where pump and probe pulses overlap, which is highlighted for the few-cycle pulse. As expected, in the nonoverlapping region no 2ω oscillations exist. The overlap region for the multicycle pulse lies between -10.7 and 10.7 fs, making the CRW oscillations visible over a larger range of delays.

To address the asymmetry of Autler-Townes splitting observed in the experiments [Fig. 2(a)], the deformation of the $4d_{5/2}^{-1}6p$ line was calculated, including only $4d_{5/2}^{-1}6p$, $4d_{5/2}^{-1}6s$ and the neutral ground state, and we find that the Autler-Townes splitting is not very asymmetric. Including additionally $4d_{5/2}^{-1}nd$ ($n = 5,6,7$) and $4d_{5/2}^{-1}ns$ ($n = 7,8$) configurations, 14 energy levels in total, the calculations resemble the asymmetric Autler-Townes splitting quite well. This strong asymmetry, where almost exclusively the upper branch of Autler-Townes splitting is seen, is due to the contributions of all the excited states.

V. CONCLUSION

In conclusion, we have shown that an intense NIR field with an intensity of 10^{13} W/cm^2 leads to CRW dynamics, which for optical pulses is on a subfemtosecond time. With attosecond transient absorption spectroscopy we time-resolve this fast dynamics, which has not been seen so far in the optical regime. The shortness of the NIR and the attosecond pulse allows for characterizing highly excited electronic states that are challenging to access with direct spectroscopic approaches due to their short lifetimes. Theoretical calculations match well with our experimental measurements and explain why the line deformation is highly asymmetric even though the excited

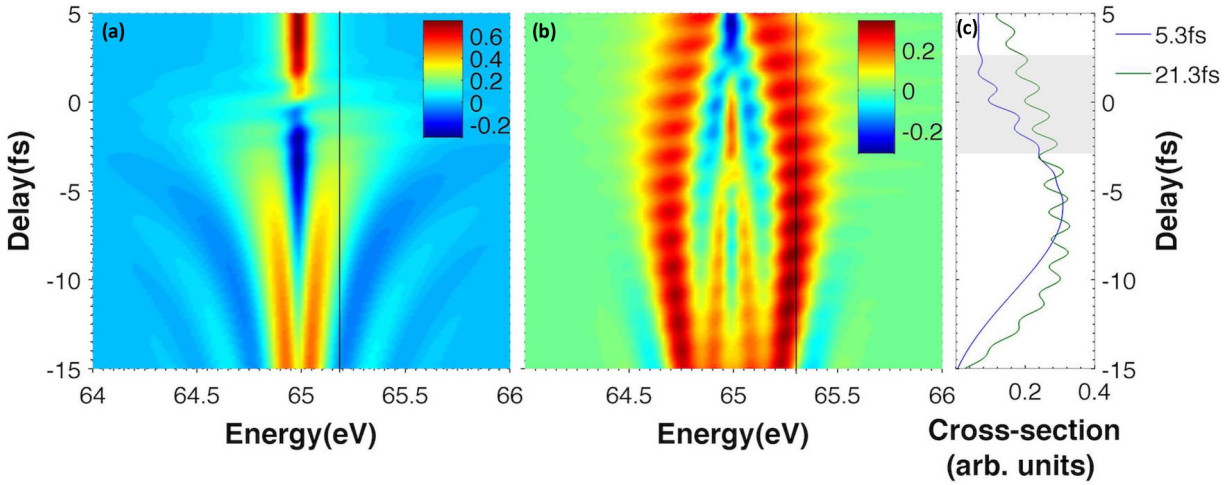

FIG. 4. CRW oscillation in the $4d_{5/2}^{-1}6p$ absorption line for different IR pulse durations**.** Calculations are done for (a) 5.3 fs (1.7 cycles) and (b) 21.3 fs (6.9 cycles) pulses. For both cases, the field strength is kept the same; namely, Ω/ω is the same. (c) The cut along an Autler-Townes branch [indicated by the black lines in (a), (b)] is shown. The amplitudes are rescaled so that they are in the same range. The 2ω oscillation (period is $\sim$1.6 fs) is clearly seen for both pulses in the overlapping region, which is highlighted in gray for the 5.3-fs pulse in (c).

electron is still bound by several eV. We could also confirm that the subcycle oscillation in the asymmetric Autler-Townes doublet is due to the CRW effects, which has been theoretically predicted. This work demonstrates the power of ATAS to observe complex electronic motion such as the electronic motion beyond the RWA approximation, which has been shown to be fundamentally important in areas such as circuit QED [13] and QC [13,14].

ACKNOWLEDGMENTS

D.K. and M.A. are supported in part by Global Research Laboratory Program (Grant No. 2009-00439) and Max Planck POSTECH/KOREA Research Initiative Program (Grant No. 2016K1A4A4A01922028) through the National Research Foundation of Korea (NRF) funded by Ministry of Science, ICT & Future Planning. S.P. is funded by the Alexander von Humboldt Foundation. This work was supported by the NSF, through a grant to ITAMP.

APPENDIX

1. Experimental setup

The atomic physics beam line at the Center for Attosecond Science and Technology (CASTECH) was used to carry out the measurements of attosecond transient absorption spectroscopy (ATAS) in xenon. We use a carrier-envelope (CE) phase-stabilized Ti:Sa laser system to produce ultrashort pulses of about 28 fs and 0.9 mJ per pulse. This pulse is first broadened using supercontinuum generation and is finally compressed to a pulse width of about 4 fs using chirped mirrors. The schematic of the beam line and absorption spectroscopy setup used in our measurements is shown in Fig. 1. The few-cycle pulse produced by the laser (4.2 fs, 800 nm, 300 μJ) is focused onto a neon gas source in a vacuum chamber to produce radiation in the XUV region by HHG.

The XUV beam along with the residual NIR then copropagates to the main experimental chamber. The NIR and the XUV pulse are then separated using a special filter consisting of a plastic pellicle (15 μm thickness) with a round metal filter (Al film) at the center. The annular NIR beam and the XUV beam at the center then fall on a two-segment curved mirror assembly. The inner segment of the mirror is a multilayered XUV mirror centered around 75 eV, having a bandwidth of about 15 eV and having a reflectivity of up to 13%. The annular-shaped outer mirror is used to reflect the NIR beam. The inner mirror can be moved relative to the outer mirror precisely using piezoelectric stages for providing the delay between the pulses. The annular outer mirror is used to reflect and focus the NIR pulse, which can be used for streaking measurements or transient absorption experiments as pump or probe pulse. The NIR intensity at the focus can be controlled using an iris placed between the special filter and the two-segment mirror assembly. The intensity of the NIR pulse is estimated using the focal spot size, the pulse width, and the energy of the pulse, and the accurate measurement of the intensity is measured by comparison of the experimental ac stark shift and the calculated shifts.

The two beams are then focused onto a quasistatic gas (xenon) cell, which is a nickel tube of 3 mm diameter with a pinhole of $\sim$100 um diameter providing an interaction length of about 2.4 mm.

The xenon gas in the gas cell is controlled using a flow controller to maintain a pressure of about 10^{-3} mbar in the target chamber. The beams are then steered using an XUV mirror and focused at the entrance slit of an XUV spectrometer using a spherical mirror. The NIR part of the beam is cut off using a 0.15-μm aluminum filter, allowing only the XUV part (64–73 eV) to the spectrometer. The XUV spectrometer consists of a slit, a spherical reflective grating (1200 lines/mm), and an x-ray CCD camera for imaging the spectrum. The spectrometer was used with XUV energies from 64 to 73 eV corresponding to the energy range of absorption for xenon. The spectrometer resolution was measured to be about 500 meV by measuring the FWHM of the $4d_{5/2}^{-1}6p$ absorption line at 65.1 eV.

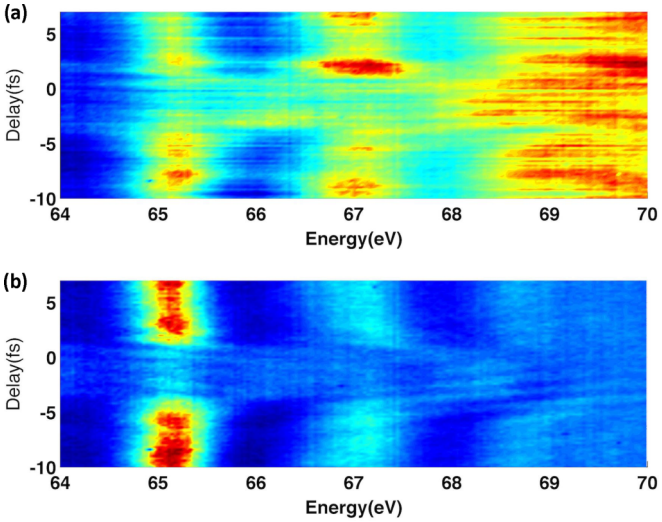

FIG. 5. (a) Raw transient absorption spectrum obtained for xenon and various delays between IR and XUV pulse. (b) The spectrum obtained after smoothening and filtering the original spectrum shown in (a).

2. Experimental data acquisition

All the measurements were obtained by measuring the transmitted spectrum (I_{gas}) through the gas target (Xe) as a function of delay (τ) between IR and XUV pulses from delays of -10 to 6 fs (negative delays corresponds to the XUV pulse arriving first) with a step of 200 as. Each measurement corresponds to an average taken over ∼9000 shots. The absorption spectrum is calculated using the reference XUV spectrum (I_0) taken in the absence of the xenon gas target. The optical density is calculated by using the following expression,

$$\mathcal{D}_{\text{opt}}(E,\tau) = \ln\left[\frac{I_{\text{gas}}(E,\tau)}{I_0}\right],$$

for each delay. The raw transient absorption spectrum is obtained by using the above expression. Such raw data contain the noises due to the fact that (1) transmitted and reference spectra were not taken simultaneously, and (2) there are always fluctuations in transmitted and reference spectra. For the quantitative analysis and the extraction of the meaningful changes, these noises were filtered out by using a Fourier method similar to one used by Ott *et al.* [29]. For each recorded XUV spectrum (containing absorption lines) at a given delay time, the spectrum was Fourier transformed and the components corresponding to the "slowly" modulating (∼3-eV period) high-harmonic XUV spectrum were filtered out. This filtered data were then inverse Fourier transformed to get $I_{\text{gas }F}(E,t)$. This filtering procedure is done for all the delays for both the transmitted and reference spectrum. The transient absorption spectrum is reconstructed using these filtered spectra, according to the equation mentioned. As a result of this filtering procedure, the statistical noise of the two-dimensional absorption spectrum is significantly reduced (see Fig. 5).

[1] S. E. Harris, J. E. Field, and A. Imamoglu, Phys. Rev. Lett. **64**, 1107 (1990).
[2] M. Fleischhauer, A. Imamoglu, and J. P. Marangos, Rev. Mod. Phys. **77**, 633 (2005).
[3] S. Ghimire, A. D. DiChiara, E. Sistrunk, U. B. Szafruga, P. Agostini, L. F. DiMauro, and D. A. Reis, Phys. Rev. Lett. **107**, 167407 (2011).
[4] A. McPherson, G. Gibson, H. Jara, U. Johann, T. S. Luk, I. A. McIntyre, K. Boyer, and C. K. Rhodes, J. Opt. Soc. Am. B **4**, 595 (1987).
[5] A. Rundquist, C. G. Durfee III, Z. Chang, C. Herne, S. Backus, M. M. Murnane, and H. C. Kapteyn, Science **280**, 1412 (1998).
[6] A. D. Shiner, B. E. Schmidt, C. Trallero-Herrero, H. J. Wörner, S. Patchkovskii, P. B. Corkum, J.-C. Kieffer, F. Légaré, and D. M. Villeneuve, Nat. Phys. **7**, 464 (2011).
[7] O. Schubert, M. Hohenleutner, F. Langer, B. Urbanek, C. Lange, U. Huttner, D. Golde, T. Meier, M. Kira, S. W. Koch, and R. Huber, Nat. Photonics **8**, 119 (2014).
[8] A. Schiffrin, T. Paasch-Colberg, N. Karpowicz, V. Apalkov, D. Gerster, S. Mühlbrandt, M. Korbman, J. Reichert, M. Schultze, S. Holzner *et al.*, Nature **493**, 70 (2013).
[9] O. Kwon, T. Paasch-Colberg, V. Apalkov, B. K. Kim, J. J. Kim, M. I. Stockman, and D. Kim, Sci. Rep. **6**, 21272 (2016).
[10] Ojoon Kwon and D. Kim, Appl. Phys. Lett. **108**, 191112 (2016).
[11] S. Pabst, D. Wang, and R. Santra, Phys. Rev. A **92**, 053424 (2015).
[12] F. Krausz and M. Ivanov, Rev. Mod. Phys. **81**, 163 (2009).
[13] T. Niemczyk, F. Deppe, H. Huebl, E. P. Menzel, F. Hocke, M. J. Schwarz, J. J. Garcia-Ripoll, D. Zueco, T. Hümmer, E. Solano *et al.*, Nat. Phys. **6**, 772 (2010).
[14] P. Forn-Díaz, J. Lisenfeld, D. Marcos, J. J. García-Ripoll, E. Solano, C. J. P. M. Harmans, and J. E. Mooij, Phys. Rev. Lett. **105**, 237001 (2010).
[15] Z. Ficek, J. Jing, and Z. G. Lu, Phys. Scr. T **140**, 014005 (2010).
[16] E. Goulielmakis, Z.-H. Loh, A. Wirth, R. Santra, N. Rohringer, V. S. Yakovlev, S. Zherebtsov, T. Pfeifer, A. M. Azzeer, M. F. Kling *et al.*, Nature **466**, 739 (2010).
[17] A. Wirth, M. Th. Hassan, I. Grguraš, J. Gagnon, A. Moulet, T. T. Luu, S. Pabst, R. Santra, Z. A. Alahmed, A. M. Azzeer *et al.*, Science **334**, 195 (2011).
[18] C. Ott, A. Kaldun, P. Raith, K. Meyer, M. Laux, J. Evers, C. H. Keitel, C. H. Greene, and T. Pfeifer, Science **340**, 716 (2013).
[19] S. Chen, M. J. Bell, A. R. Beck, H. Mashiko, M. Wu, A. N. Pfeiffer, M. B. Gaarde, D. M. Neumark, S. R. Leone, and K. J. Schafer, Phys. Rev. A **86**, 063408 (2012).
[20] H. Wang, M. Chini, S. Chen, C.-H. Zhang, F. He, Y. Cheng, Y. Wu, U. Thumm, and Z. Chang, Phys. Rev. Lett. **105**, 143002 (2010).
[21] M. Schultze, K. Ramasesha, C. D. Pemmaraju, S. A. Sato, D. Whitmore, A. Gandman, J. S. Prell, L. J. Borja, D. Prendergast, K. Yabana, D. M. Neumark, and S. R. Leone, Science **346**, 1348 (2014).
[22] M. Wu, S. Chen, M. B. Gaarde, and K. J. Schafer, Phys. Rev. A **88**, 043416 (2013).
[23] A. N. Pfeiffer and S. R. Leone, Phys. Rev. A **85**, 053422 (2012).

[24] S. Pabst, A. Sytcheva, A. Moulet, A. Wirth, E. Goulielmakis, and R. Santra, Phys. Rev. A **86**, 063411 (2012).
[25] L. Greenman, P. J. Ho, S. Pabst, E. Kamarchik, D. A. Mazziotti, and R. Santra, Phys. Rev. A **82**, 023406 (2010).
[26] S. Pabst, Euro. Phys. J. Spec. Top. **221**, 1 (2013).
[27] S. Pabst and R. Santra, Phys. Rev. Lett. **111**, 233005 (2013).
[28] S. Chen, M. Wu, M. B. Gaarde, and K. J. Schafer, Phys. Rev. A **87**, 033408 (2013).
[29] C. Ott, A. Kaldun, L. Argenti, P. Raith, K. Meyer, M. Laux, Y. Zhang, A. Blättermann, S. Hagstotz, T. Ding *et al.*, Nature **516**, 374 (2014).
[30] X. Wang, M. Chini, Y. Cheng, Y. Wu, X.-M. Tong, and Z. Chang, Phys. Rev. A **87**, 063413 (2013).
[31] G. M. Genkin, S. E. Razov, and A. G. Razov, Opt. Spectrosc. **91**, 9 (2001).
[32] J. Tuorila, M. Silveri, M. Sillanpää, E. Thuneberg, Y. Makhlin, and P. Hakonen, Phys. Rev. Lett. **105**, 257003 (2010).
[33] T. E. Glover, M. P. Hertlein, S. H. Southworth, T. K. Allison, J. van Tilborg, E. P. Kanter, B. Krässig, H. R. Varma, B. Rude, R. Santra *et al.*, Nat. Phys. **6**, 69 (2010).
[34] C. Buth, R. Santra, and L. Young, Phys. Rev. Lett. **98**, 253001 (2007).